Submillimetre HCO^+ observations of warm cloud cores: the excitation of molecular lines in dense star formation regions

Astron. Astrophys. 198, 237–248 (1988)

ASTRONOMY
AND
ASTROPHYSICS

Submillimetre HCO^+ observations of warm cloud cores: the excitation of molecular lines in dense star formation regions

K.J. Richardson[1], Glenn J. White[1], T.S. Monteiro[2,★], and Saeko S. Hayashi[3,★★]

[1] Department of Physics, Queen Mary College, Mile End Road, London E1 4NS, England
[2] School of Physics, The University, Newcastle-upon-Tyne NE1 7RU, England
[3] Nobeyama Radio Observatory, Nobeyama, Minamisaku, Nagano 384-13, Japan

Received June 17, accepted November 19, 1987

Summary. We have made submillimetre wavelength observations towards the cores of the molecular clouds S 255, DR 21, DR 21(OH), OMC-2 and Mon R2, in the $J = 4 - 3$ transitions of HCO^+ and $H^{13}CO^+$, in order to investigate their spatial and velocity structure. In the case of Mon R2 these have been supplemented by additional higher angular resolution ($\sim 15''$–$20''$) observations in the $J = 1 - 0$ lines of HCO^+, HCN and CO. Particular features of the data obtained include the detection of an asymmetrical self-reversed profile for the HCO^+ $J = 4 - 3$ line towards the centre of DR 21(OH). This may be due to a collapsing cloud core, or alternatively a foreground absorbing cloud with a line-of-sight velocity component directed towards the cloud centre. In addition, we detect a double peaked structure associated with the centre of the molecular outflow in Mon R2. This is consistent with a central rotating disc.

In general, the observed line profiles towards these sources suggest the presence of small scale fragmentation (clumping) in the densest regions on scales of ~ 0.1 pc. These data are analysed in conjunction with submillimetre wavelength continuum measurements at $\lambda = 370\,\mu$m, which are used to estimate average gas densities. Hence, combined spatial and velocity dilution factors are derived, together with values for the relative abundance of HCO^+. The dilution factors have a fairly invariant value of ~ 0.1 for all sources. The estimated relative molecular abundances estimated for Mon R2 and DR 21 are an order of magnitude higher than those for the other sources observed. We discuss the radiative transfer conditions and possible alternative mechanisms for excitation of the HCO^+ $J = 4 - 3$ transition. It is shown that values for derived molecular abundances are sensitive to the details of the radiative transfer model used, discrepancies of up to an order of magnitude occurring between the results derived from the two alternative models considered. We predict however that for a wide range of likely clump parameters, high resolution submillimetre molecular line profiles should be self reversed, and future observations of qualitative features of line profiles should enable a choice to be made between alternative radiative transfer models. In addition to the normally considered HCO^+/ground state H_2 collisional excitation mechanism, excitation by collisions with rotationally excited H_2, radiative excitation via the infrared continuum radiation field and excitation by ambipolar drift are discussed as possible excitation mechanisms.

Key words: molecular clouds – interstellar molecules – radiative transfer

1. Introduction

Molecular line observations provide a powerful means of probing the conditions within dense star formation regions. They contain both spatial and velocity information and the large number of rotational transitions observable covers a wide range of excitation conditions. However, many observations carried out in recent years have shown the dense cores of molecular clouds to be complex and inhomogeneous. This can make the unique interpretation of molecular line data difficult, because of unknown radiative transfer effects and uncertainties of the filling factors within telescope beams. As a result, estimated H_2 densities and relative molecular abundances can be highly model dependent. Accurate estimates of molecular abundances are needed to test the predictions of cloud chemistry models. Moreover, such models sometimes predict variations of the relative molecular abundance between the dense and less dense regions within a given cloud. This is because of the time scale of $\sim 10^9/n_{H_2}$ yr for the condensation of molecules onto grains (Williams, 1986), and also of local processes such as shocks and photodissociation. Data in the millimetre and submillimetre continuum can provide a useful additional source of information since, unlike most line observations, they are usually optically thin at these wavelengths, and are therefore relatively unaffected by radiative transfer effects.

We have made observations of a small number of molecular cloud cores in the $J = 4 - 3$ transitions of HCO^+ and $H^{13}CO^+$. These lines are thought to be excited in the denser regions inside the cores of clouds. Our source list consists of objects which fall

Send offprint requests to: K.J. Richardson
★ Present address: Department of Physics, University of Durham, Science Laboratories, South Road, Durham, DH1 3LE, England
★★ Present address: James Clerk Maxwell Telescope Section, United Kingdom Telescope Unit, 665 Komohana Street, Hilo, Hawaii 96720, USA

into the category of warm-centred clouds, in the nomenclature of Evans (1978). Our initial objective has been to map the spatial and velocity structure of the regions with a view to understanding their morphology. However, attempts to model the data lead us to consider in more detail the radiative transfer and line excitation mechanisms which may be important. The data are presented and discussed below, in conjunction with 370 μm continuum data and, in the case of the source Mon R2, with additional data in the $J = 1 - 0$ lines of HCO^+, HCN and CO.

2. Observations

The submillimetre molecular line observations were made with the 3.8 m United Kingdom Infrared Telescope (UKIRT), mostly during November 1985. The instrument used was the Queen Mary College Submillimetre wavelength Spectral Line Receiver (White et al., 1981; White et al., 1986). All the data are presented in terms of the quantity T_r^*, calibrated using the standard chopper wheel method (Kutner and Ulich, 1981), with the forward spillover efficiency η_{fss} being estimated as 0.9. The beam size (FWHM) was 55″. The velocity resolution was 0.5 km s^{-1}, apart from for OMC 2, where it was 0.33 km s^{-1}.

The $J = 1 - 0$ line observations towards Mon R2 were obtained in April 1985 using the Nobeyama 45 m telescope, which has a beamwidth of 20″ at the frequency of the HCO^+ and HCN $J = 1 - 0$ transitions and 15″ at the frequency of the CO $J = 1 - 0$ line. Mapping observations were carried out simultaneously in the HCO^+, HCN and CO $J = 1 - 0$ lines, using a polarisation splitter to send orthogonal polarisations into two different receivers, which operated in the respective frequency bands. The spectra were processed using a 2 GHz bandwidth AOS back-end. The weather and atmospheric transparency during this period was poor. Because of this, and also the greatly different beamsize and antenna power pattern compared with UKIRT, we attempt no quantitative comparison between the two data sets, but simply consider the qualitative features of the data which we believe to be significant.

A brief description of the data for each source follows:

2.1. OMC-2

This source, which was first observed at infrared wavelengths by Gatley et al. (1974), has been observed in the CO $J = 1 - 0$ transition by Fischer et al. (1985), who detected a SW–NE bipolarity in the line wings, attributing it to an outflow. The source has also been detected in lines of shocked molecular hydrogen (Thronson and Thompson, 1982).

The HCO^+ $J = 4 - 3$ observations of OMC-2 are shown in Fig. 1. The peak intensity varies smoothly over the extent of the map, but there are significant variations in profile shape from one position to the next. In particular, broader linewidths are seen at the $(-30'', -30'')$ and $(30'', 30'')$ positions, together with a bipolarity in the blue (NE) and red (SW) wings. This is similar in orientation to that observed by Fischer et al. (1985) in the CO $J = 1 - 0$ line. The $H^{13}CO^+$ $J = 4 - 3$ line is not significantly detected at the (0, 0) position, but weak emission is detected at the $(30'', 30'')$ position, the velocity centre of which is offset by -2 km^{-1} relative to that of the HCO^+ line. Apart from this bipolarity, there are also significant variations in profile shapes between adjacent grid points. This suggests the existence of small scale structure in the source on scales $\lesssim 0.1$ pc.

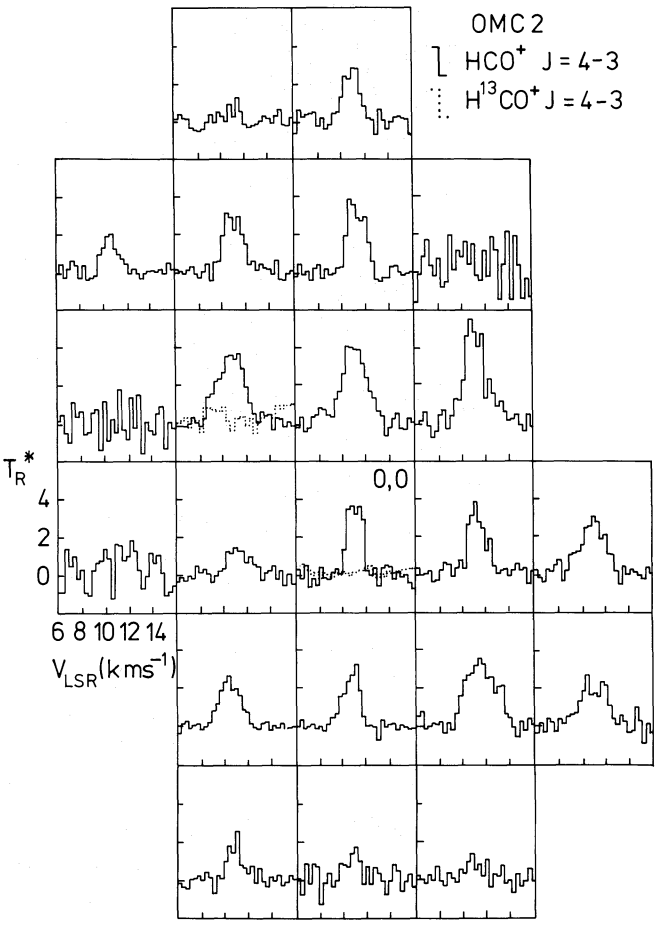

Fig. 1. Mapping of OMC 2 in the $J = 4 - 3$ transitions of HCO^+ and $H^{13}CO^+$. The (0, 0) position is α (1950) $05^h32^m59^s$; δ (1950) $-05°12'00''$, and the grid spacing is 30″, corresponding to a distance of ~ 0.07 pc

2.2. Mon R2

The line profiles over the central region of this source, shown in Fig. 2a, are much more invariant than for OMC-2. Emission in the isotopic line $H^{13}CO^+$ was detected towards the positions (0, 0) and $(-30'', -30'')$, with $\sim 30\%$ of the HCO^+ integrated intensity.

The HCO^+, HCN and CO $J = 1 - 0$ data observed at Nobeyama are shown in Figs. 2b–e. These maps of integrated intensity over velocity intervals around the line centre exhibit a double structure in all three lines, though this is not very pronounced in the HCO^+ map. (Note that the velocity intervals for the maps are not quite identical. However, since we are only considering the general morphology, this should not give rise to serious error.) The two peaks are separated by $\sim 2'$, corresponding to ~ 0.5 pc for an assumed source distance of 830 pc. In the case of the HCN transition, the line joining the two peaks is approximately orthogonal to the axis of the molecular outflow in Mon R2 (Loren 1981). There is also a gradient in the velocity of peak intensity along the line joining the two peaks. This is shown in Fig. 2e for HCO^+ and HCN. The HCN emission

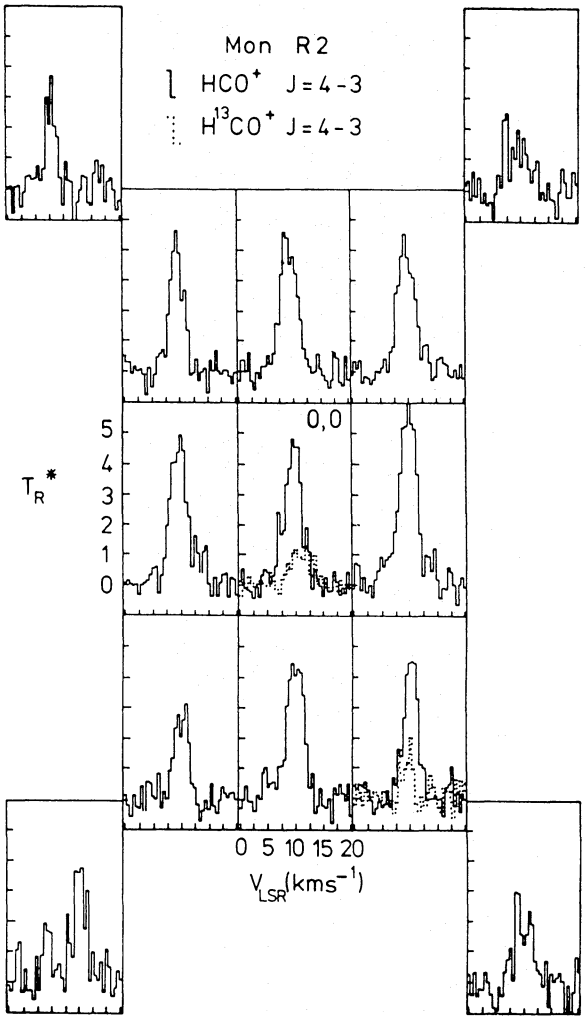

Fig. 2a. Mapping of Mon R2, in the HCO^+ and $H^{13}CO^+$ $J = 4 - 3$ transitions. Grid reference position α (1950) $06^h05^m21^s$; δ (1950) $-06°22'28''$. Otherwise same as Fig. 1

has an average velocity gradient in the plane of the sky of $\sim 1.7\,\mathrm{km\,s^{-1}\,pc^{-1}}$. For this velocity gradient and separation between the peaks, a total mass of $\sim 150\,M_\odot$ would be implied for gravitational binding. From the observed 370 μm continuum flux (see Table 2) and using the method described by Hildebrand (1983) we estimate the total mass within a 55″ beam to be $\sim 190\,M_\odot$. Given the likely sources of error in both these estimates, the HCN observations considered in isolation are therefore consistent with a gravitationally bound disk-like structure or binary system. However, this interpretation is tentative because the orientations and qualitative appearances of the double peaked structures vary somewhat between transitions.

In most positions, the peak intensities in the HCO^+ and HCN $J = 1 - 0$ lines are within $\sim 20\%$ of each other, although at a few particular positions e.g. (+60″, +40″), (+60″, +20″) and (−60″, −40″) the HCN line appears to be $\sim 50\%$ stronger. This has the effect of making the HCN maxima appear more compact, while the peaks seen in HCO^+ appear somewhat extended along the direction of the outflow. We note further that over some of the map the velocity of peak HCN intensity is greater by up to $0.7\,\mathrm{km\,s^{-1}}$ than that of HCO^+. This effect is most pronounced around position −60″, 0 (see Fig. 2b).

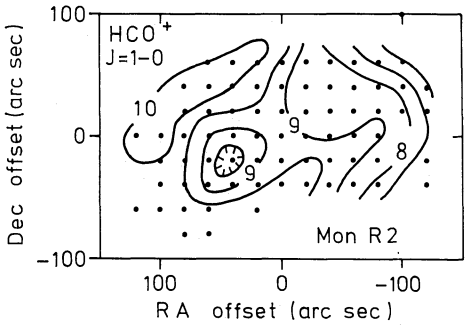

Fig. 2b. Mapping of Mon R2 in the HCO^+ $J = 1 - 0$ transition. The contours are of integrated T_A^* ($\mathrm{K\,km\,s^{-1}}$) between 8 and $12\,\mathrm{km\,s^{-1}}$. To convert to integrated T_R^* these values should be divided by $\eta_{fss} \sim 0.4$, although due to the complexity of the source, uncertain antenna pattern and very poor weather conditions, the absolute intensities are uncertain to at least 50%. Contour levels 6, 7, 8, 8.5, 9, 9.5, $10\,\mathrm{K\,km\,s^{-1}}$. The data positions are indicated by dots

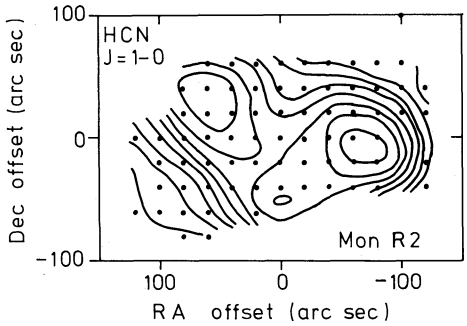

Fig. 2c. Mon R2, HCN $J = 1 - 0$, velocity interval 5 to $18\,\mathrm{K\,km\,s^{-1}}$. Contours from 7 to $23\,\mathrm{K\,km\,s^{-1}}$ in steps of 2. Otherwise the same as Fig. 2b

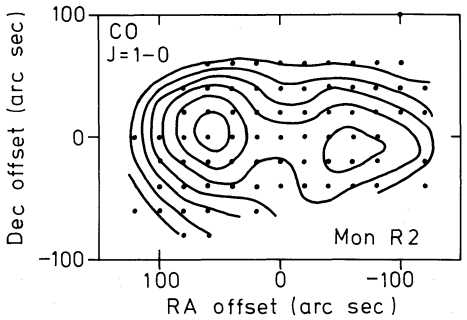

Fig. 2d. Mon R2, CO $J = 1 - 0$, velocity interval 10 to $12\,\mathrm{K\,km\,s^{-1}}$. Contours from 11 to $23\,\mathrm{K\,km\,s^{-1}}$ in steps of 2. Otherwise the same as Fig. 2b

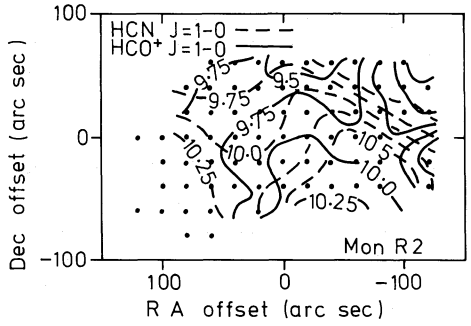

Fig. 2e. Mon R2, velocity ($\mathrm{km\,s^{-1}}$) of peak intensity for the HCO^+ and HCN $J = 1 - 0$ transitions

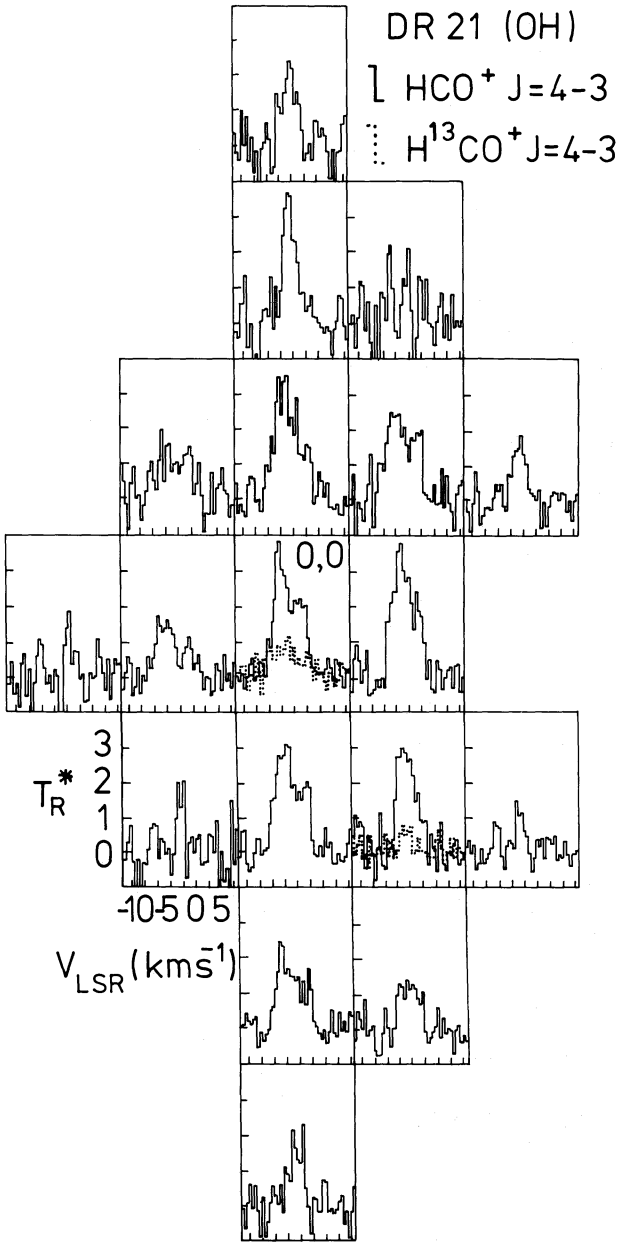

Fig. 3. Mapping of DR 21(OH). Grid reference position α (1950) $20^h37^m14^s$; δ (1950) $+42°12'00''$. Otherwise same as Fig. 1

2.3. *DR 21 (OH)*

Our previous observations of this source were presented and discussed in Richardson et al. (1986), referred to throughout the rest of this paper as Paper I. The present HCO^+ $J = 4 - 3$ data are presented in Fig. 3.

The variations in profile shape over this source are relatively smooth, although, since it lies at a greater distance ($\sim$3 kpc) compared with our other sources, any small scale structure would be correspondingly more difficult to discern. The most striking feature of the map is the prominent self-reversal seen towards (0, 0) and some adjacent positions. The centre of the reversal is redshifted with respect to the velocity of peak intensity. No such feature is seen in the $H^{13}CO^+$ transition, which peaks within the HCO^+ self reversal, but otherwise has a similar shape to that of

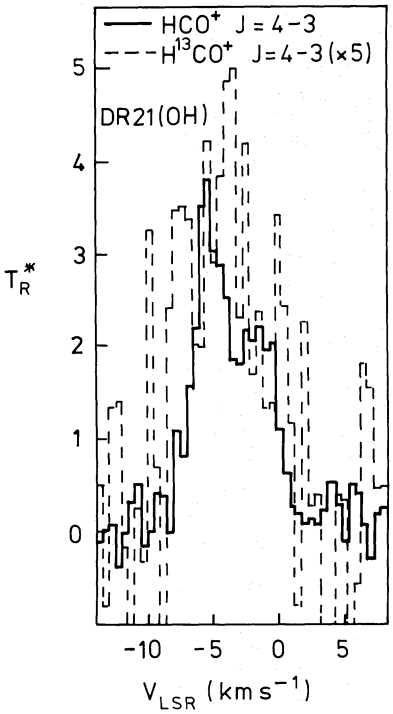

Fig. 4. HCO^+ and $H^{13}CO^+$ $J = 4 - 3$ spectra of DR 21(OH) (0, 0) position. The $H^{13}CO^+$ intensity has been multiplied by 5

the more abundant isotope (see Fig. 4). The absence of a self-reversal in the line of the less abundant isotope indicates that its presence in the HCO^+ line may be a radiative transfer effect rather than due to separate emitting clouds of gas along the line of sight. One possible explanation for the self-reversal and the sense of its asymmetry would be the existence of a systematic radial *inflow*, with radiation from the centre of the cloud core being absorbed over redshifted velocities by infalling material further out (see Figure 9(c) below for an example of this phenomenon). An alternative possibility would be a foreground absorbing cloud which had a velocity component towards the cloud centre.

2.4. *S 255 and DR 21*

Observations of these sources in the HCO^+ $J = 4 - 3$, $H^{13}CO^+$ $J = 4 - 3$, and other transitions have been presented and discussed by Richardson et al. (1985) and in Paper I, but are relevant to the general discussion of this paper also. For both sources, the $H^{13}CO^+$ and HCO^+ profiles have similar shapes and widths and none is self reversed.

3. Discussion

The general plan of the discussion is as follows. We first summarise the main common features of the observations and discuss simple modelling which yields some insight into the structure of and conditions within these cloud cores. We then consider in more detail the radiative transfer problem and the implications for various derived parameters. Finally, we attempt a comparative assessment of some alternative excitation mechanisms for the HCO^+ $J = 4 - 3$ transition.

Table 1. Molecular line results

Source	$\int T_R^* dV$ $H^{13}CO^+$ $J=4-3$ (K km s^{-1})	$\int T_R^* dV$ HCO^+ $J=4-3$ (K km s^{-1})	R_{int}	ΔV FWHM HCO^+ (km s^{-1})	η_c	F	$N_{H^{13}CO^+}$ ($\times 10^{11}$ cm^{-2})
S 255	1.2	8.5	6.9	4	0.8	0.06	4.9
DR 21	7.0	37.0	5.3	12	0.6	0.11	37.7
DR 210H	6.1	20.2	3.3	7.5	0.8	0.10	23.3
Mon R2	5.0	18.2	3.6	5	0.8	0.09	20.7
OMC 2	0.5	6.3	11.9	2	0.8	0.11	2.0
OMC 1	44.9	193.9	4.3	8	0.9	0.26	234.0

3.1. General discussion and simple modelling

The following general features are apparent in the data:

Firstly, the ratio R_{int} of integrated intensities, defined by

$$R_{int} = \frac{\int T_r^*(HCO^+ J=4-3)\,dV}{\int T_r^*(H^{13}CO^+ J=4-3)\,dV} \quad (1)$$

is in general $\lesssim 10$ (see Table 1), which is much less than the usually assumed isotopic abundance ratios which lie in the range 40–90. *This implies that the $J=4-3$ HCO^+ transition is optically thick.* A possible exception is the (0, 0) position for OMC-2, where the data are consistent with optical thinness. As argued by Richardson et al. (1985) for the case of S 255, isotopic fractionation effects, which might provide an alternative explanation for the observed intensity ratios, are probably unimportant here.

Secondly, for most of the positions observed in both isotopic lines, the HCO^+ and $H^{13}CO^+$ profiles have similar widths and shapes, none except the HCO^+ spectrum towards DR 21 (OH) showing signs of self reversal. However, we note that for some positions in OMC-2 and Mon R2, the velocities of the line peaks show differences of up to 2 km s^{-1} between the two isotopic species.

We next address the question of which radiative transfer model best represents the cloud structures. We note at the outset that one might expect to see qualitative differences between line profiles for two transitions having very different optical depths, since the spectra would sample conditions at different points within the cloud. Also, since velocities further towards the edges of a spectral line profile sample emission from greater distances into a cloud (White, 1977), self reversed profiles are expected in cases where the excitation temperature increases towards the centre. This situation may well occur even for a homogeneous cloud of constant temperature and density, because of the greater photon escape probability near the edge. In fact, modelling of microturbulent clouds does often predict the occurrence of broad, deep and spatially extended self absorptions in the HCO^+ $J=4-3$ transition (Richardson, 1985). However, such features are noticeably absent from the present data. Simple collapse models of clouds, utilising the large velocity gradient (LVG) approximation (Goldreich and Kwan, 1974), can easily produce similar profile shapes without self absorptions for lines of different optical depths. However, the predicted absolute intensities from such models tend to conflict with the observed values. This is because for observed values of R_{int} typical of the sources in our sample, an excitation temperature is predicted for the HCO^+ $J=4-3$ transition which is typically $>50\%$ of the kinetic temperature (as estimated either from continuum photometry or CO observations). This is in conflict with the typical observed values of $\sim 10\%$.

In view of the inability of either of these idealised models to reproduce the main features of the data, we are led to consider a model consiting of many small clumps, as was discussed in Paper I. This is capable of reproducing the observed qualitative aspects of the profiles, since the profile shapes are mainly determined not by the structure of an individual clump, but by the relative velocities between clumps. The low absolute intensities of the HCO^+ lines are then readily accounted for in terms of beam dilution i.e. the concentration of most of the cloud material into fragments which only partly fill the beam and are unresolved both spatially and kinematically. The similarities in line profile shapes between different isotopes can also be understood since, although more than one clump may exist along any given direction, they will in general have different line-of-sight velocities and will not absorb each other's emitted radiation. Consequently, it is possible to see right through a dense cloud core even in an optically thick line, although the absolute observed intensity may then consist mainly of contributions from only the surface layers of individual clumps. *If this is the case, future higher spatial resolution observations in these submillimetre transitions might be expected to reveal self reversals towards individual fragments which are diluted out by larger telescope beams.* (Note, however, that such self-reversals tend not to be predicted in the $J=1-0$ transitions which we have observed with the Nobeyama telescope, as discussed below.)

We will now carry out an initial assessment of the data, in order to account for the general trends mentioned above, before then considering the limitations of this preliminary treatment and the reasons for the individual characteristics of the data for each source.

We consider a very simple cloud model consisting of a number of identical, homogeneous clumps. This is similar to that developed in Paper I, to which the reader is referred for further details. We define a dilution factor F by

$$F = \frac{\int T_r^*(HCO^+ J=4-3)\,dV}{T_{ex}(1-e^{-\tau})\,\Delta V\,\eta_c} \quad (2)$$

where T_{ex} is the excitation temperature of the transition, assumed equal to the kinetic temperature as estimated from continuum photometry, ΔV is the total line width (FWHM) and η_c is the beam coupling efficiency onto the region (Kutner and Ulich, 1981). The optical depth τ is assumed to be $\gg 1$. The factor F is

also given in terms of the clump properties by

$$F = \frac{N\,\Delta v_c\, r^2}{\Delta V R^2} \tag{3}$$

where r and Δv_c are the radius and velocity width of an individual clump, R is the radius of the region contained within the beam, and N is the total number of clumps in the beam.

Values of F calculated from (2) are shown in Table 1. They have a fairly invariant value of ~ 0.1, for regions having a range of different total luminosities and physical dimensions. The fact that $F \ll 1$ provides some retrospective justification for the basic model, since with such a low value one would indeed expect to see right through the regions.

Assuming appropriate values for the clump size and velocity width, we can use (3) to make an order-of-magnitude estimate of N. Since this is very sensitive to the values adopted, we have not tabulated individual estimates, but typical derived numbers, assuming thermal velocity widths and Jeans length sized clumps, are of order 10^0 for OMC 2, 10^1 for Mon R2, S 255 and OMC 1, and 10^2 for DR 21 and DR 21(OH).

3.1.1. Optically thin analysis

From the $H^{13}CO^+$ data, a lower limit can be placed on the value of X_{HCO^+}, the abundance of HCO^+ relative to H_2. To do this, we have combined the molecular line observations with submillimetre wavelength continuum data, which can be used to derive average H_2 densities (e.g. see the review by Hildebrand, 1983). The details of the analysis are essentially similar to that used in Paper I. We have used 370 μm continuum observations which were obtained with beam sizes as similar as possible to our 55″ beam. For both the line and continuum data we have for convenience adopted a simplified assumed beam profile, in which the antenna response pattern was taken to be uniform within a 55″ diameter circle but zero outside that.

The continuum data used (either our own or taken from the literature), and the estimated H_2 column densities N_{H_2}, are summarised in Table 2. Also tabulated are the average H_2 densities, $\bar{n}_{H_2}$, derived on the assumption that the line-of-sight extent of the sources' dense molecular cores are similar to their observed 370 μm sizes. The density n_{H_2} within the clumps is then given by the relationship

$$n_{H_2} = \bar{n}_{H_2} R^3/(Nr^3). \tag{4}$$

The integrated $H^{13}CO^+$ $J = 4 - 3$ intensities were used to derive molecular column densities $N_{H^{13}CO^+}$, assuming the $H^{13}CO^+$ $J = 4 - 3$ transition to be optically thin and thermalised to the dust kinetic temperature T_D. The results are given in Table 1. Dividing these values by the estimated H_2 column densities and assuming an isotopic abundance ratio of 40, we obtain for each source a lower limit for X_{HCO^+}. These results, which are presented in Table 3, have the advantage of being derived *purely from optically thin data.* In addition, they are values *characteristic of the dense clumps* and not contaminated by emission and absorption in less dense inter-clump or foreground material. *They are, however, likely to be severe lower limits,* partly because the $H^{13}CO^+$ emission may have an optically thick contribution, but more importantly because this isotopic line may not be totally thermalised to the gas kinetic temperature over all the 370 μm emitting region.

3.2. Radiative transfer and model-dependence of derived quantities

To obtain particular values, rather than just lower limits, for X_{HCO^+}, it is necessary to make some assumptions about the kinematical structure of individual clumps, since these will affect the radiative transfer. Given a suitable model, and assumed values for all the relevant cloud parameters and the isotopic abundance ratio, it is possible to predict a value for R_{int}, which can be compared against the observed value. In the particularly simple case of the LVG approximation, any assumed H_2 density, n_{H_2}, gives a unique solution for the quantity $X_{HCO^+}/(dV/dR)$, the abundance of HCO^+ relative to H_2 per unit local gas systematic velocity

Table 2. Continuum results

Source	S_{370} Jy (55″ beam)	T_D (K)	Source dist. (kpc)	Source size 370 μm (arcmin)	τ_{370}	N_{H_2} (10^{23} cm^{-2})	$\bar{n}_{H_2}$ (10^5 cm^{-3})	Refs[d]
S 255	380	44	2.5	0.9	0.04	2.2	1.0	1, 1, 1
DR 21	870	47[b]	3.0	0.9	0.08	4.3	1.8	2, 6, 2
DR 21 OH	1290	35[b]	3.0	0.8	0.24	12.4	5.5	2, 6, 2
Mon R2	560	50	0.83	2.5	0.05	2.5	1.3	3, 7, 3
OMC 2	370[a]	38[c]	0.5	5.0	0.05	2.9	1.3	4, 8, 5
OMC 1	5600	100	0.5	3.0	0.15	7.7	5.7	1, 9, 5

[a] 390 μm flux in 1′25 beam.
[b] Also in good agreement with more recent mapping by Harvey et al. (1986).
[c] Gas temp from CO $J = 1 - 0$ data of Fischer et al. (1985) and our own unpublished data. Continuum data (Ref. 5) gives 30 K.
[d] Refs. refer respectively to S_{370}, T_D, Source size (370 μm)
References: (1) Richardson et al. (1985); (2) Paper I; (3) Cunningham, 1982, Ph.D. thesis; (4) Thronson et al. (1978); (5) Smith et al. (1979); (6) Harvey et al. (1977); (7) Thronson et al. (1980); (8) Fischer et al. (1985); (9) Wynn Williams et al. (1984)

Table 3. Derived abundances

Source	Optically thin X_{HCO^+} (lower limit)	Model 1		Model 2	
		n_{H_2} (10^6 cm^{-3})	X_{HCO^+}	n_{H_2} (10^6 cm^{-3})	X_{HCO^+}
S 255	$9.0\,10^{-11}$	1.8	$1.1\,10^{-10}$	.74	$6.8\,10^{-10}$
DR 21	$3.5\,10^{-10}$	1.5	$1.0\,10^{-9}$	.27	$6.6\,10^{-9}$
DR 21 OH	$7.5\,10^{-11}$	5.0	$8.5\,10^{-11}$	1.4	$1.0\,10^{-9}$
Mon R2	$3.4\,10^{-10}$	1.6	$1.6\,10^{-9}$	.45	$5.6\,10^{-9}$
OMC 2	$2.8\,10^{-11}$	1.3	$1.9\,10^{-10}$	1.1	$1.6\,10^{-9}$
OMC 1	$1.2\,10^{-9}$				

gradient, if the gas kinetic temperature T_K and the value of R_{int} are estimated from observations. White (1977) calculated the predicted antenna temperatures for the lowest two CO transitions from both LVG and microturbulent models, and concluded that predicted intensities from the alternative models agreed within factors attributable to ignorance of the cloud geometry. The implication of this result would be that it is safe to use the computationally convenient LVG assumption in deriving cloud parameters from molecular line data, even though LVG models are not now thought to give a true physical representation of actual cloud dynamics.

But the discussion by White (1977) was restricted to homogeneous clouds which were implicitly assumed to be well resolved by the telescope beam. It is not immediately apparent how his result would carry over to the case of integrated intensities from beam diluted clumps, since the apparent size of a clump might be expected to change across the line profile, and also to vary between transitions.

Consequently, in order to assess the model dependence of the derived quantities we have considered two alternative models for the clumps. To keep the computing requirements within reasonable bounds, we have restricted the modelling to a kinetic temperature of 40 K, which is within 20% of the derived dust temperature of all the observed sources except OMC 1. Both models make use of the results for average density (see Table 2) obtained from the continuum data, which is assumed to be optically thin.

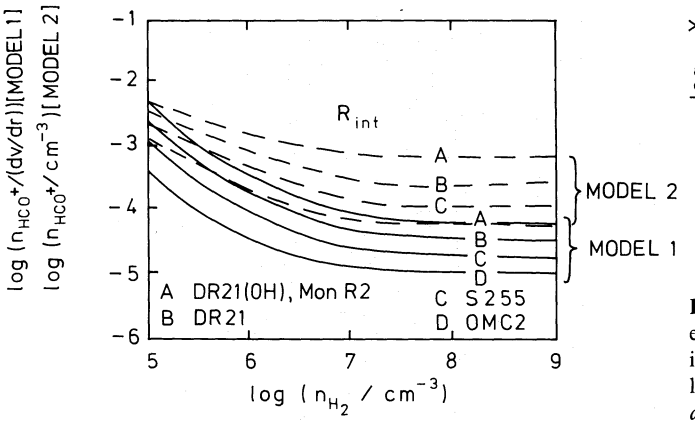

Fig. 5. Contours corresponding to the observed line intensity ratios R_{int} for Models 1 (solid lines) and 2 (broken lines). See text for details

Model 1: This is the basic LVG model which was used, and is described in more detail, in Paper I. Essentially, an LVG program was used to plot contours of R_{int} on axes of n_{H_2} and $n_{HCO^+}/(dV/dR)$, where n_{HCO^+} is the number density of the formyl ion. This is shown in Fig. 5 for the observed R_{int} of each source. We have considered a range of possible values for the gas density n_{H_2} within the clumps. For each value of assumed density $> \bar{n}_{H_2}$, Eqs. 3 and 4 are solved for $\Delta v_c/2r$ – this is taken as an estimate of dV/dR. Then, using Fig. 5, one obtains a value for n_{HCO^+} and hence X_{HCO^+}.

The range of solutions for X is shown in Fig. 6 for each source. The lower limit for n_{H_2} is the mean density, $\bar{n}_{H_2}$. The upper limit is fixed by assuming that dV/dR for a given n_{H_2} cannot be greater than would be given by unimpeded free-fall collapse. These limits are sufficient to constrain the value of X_{HCO^+} to within an order of magnitude for each source. Particular values for X_{HCO^+} are obtained if it is assumed that dV/dR for a clump can be approximated by $\Delta V/2R$, the total line width divided by the diameter of the source. These are shown in Table 3 (together with the corresponding values of n_{H_2}) and are in excess of the

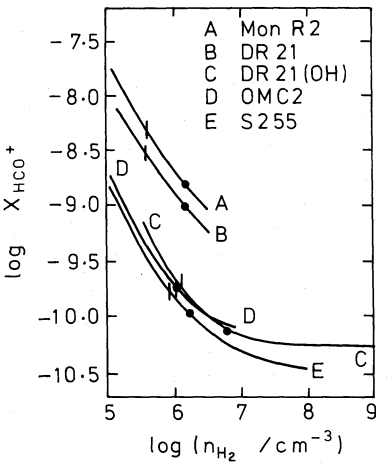

Fig. 6. Range of solutions for X_{HCO^+} according to Model 1. The total extent of each curve is fixed by the absolute limits on n_{H_2} as described in the text. The point on the curve for each source where the solution lies is fixed by specifying the value of dV/dR. The filled circles are for $dV/dR = \Delta V_{FWHM}$/Source size; these are the Model 1 solutions given in Table 3. The vertical tick marks are for $dV/dR = 2.5\,\mathrm{km\,s^{-1}\,pc^{-1}}$ c.f. clump parameters of model 2

previously derived lower limits by factors in the range 1.1 (DR 21 OH) to 6.8 (OMC 2).

Model 2: Here we have considered a cloud core consisting of identical homogeneous clumps of diameter 0.1 pc, having a kinetic temperature of 40 K, with no systematic velocity gradients within a clump, but with a microturbulent velocity width (FWHM) of 0.25 km s^{-1}, this being the thermal velocity width of HCO^+ molecules at a kinetic temperature of 40 K. The emission in the $J = 4 - 3$ transitions of both HCO^+ and $H^{13}CO^+$ was computed for a single clump, using a Monte Carlo radiative transfer program (Avery, 1983). This was repeated for a grid of assumed H_2 densities and values of X_{HCO^+}. It was assumed that the radiative transfer in a clump is unaffected by radiation from other clumps, and can therefore be treated independently. This should be a valid approximation for $F \ll 1$, as is the case for these sources. The predicted intensities were then integrated over the spatial extent of the clump and across the line profiles, leading to predicted values of R_{int} for the beam-diluted clumps. Contours of R_{int} corresponding to the observed values for each source are shown in Fig. 5, on axes of n_{H_2} and n_{HCO^+}.

In this case too, we have a range of possible solutions for n_{H_2} and n_{HCO^+}. The assumed values of $\Delta v_c = 0.25$ km s^{-1} and $r = 0.05$ pc are in this case sufficient, using Eqs. (2) and (3) in conjunction with the data presented in Table 1, to fix a value for n_{H_2} and hence to deduce X_{HCO^+}. The values of X_{HCO^+} determined in this way are given in Table 3, again with the corresponding values of n_{H_2}.

The salient feature of the results summarised in Table 3 is the wide discrepancy between the relative abundances given by models 1 and 2, those from model 2 being up to an order of magnitude higher. Direct comparison is in fact not straightforward, because of the different parameters which need to be specified independently in the two models. This is because of the global nature of the radiative transfer within a clump in the case of model 2, which require values for the size and velocity width of the clumps (neither observable directly with our beam size) to be assumed. It is therefore possible that some of the discrepancy between the models could be accounted for:

(1) By the differences between the estimates for n_{H_2} (see Table 3);

(2) Because the total velocity width divided by source diameter (used as an estimate for dV/dR in model 1) differs from the corresponding quantity for a single clump, $\Delta v_c/2r$ ($= 2.5$ km s^{-1} pc^{-1}) used in model 2.

Within the context of model 1, these quantities are not independent; they are constrained by the observed value of F and the mean gas density $\bar{n}_{H_2}$ derived from the 370 μm fluxes (see Eqs. 3 and 4). In Fig. 6, we show the solutions for X_{HCO^+} which would be obtained from model 1, for $dv/dr = 2.5$ km s^{-1}, corresponding to the assumed clump parameters of model 2. From Fig. 6, we see that the estimated model 1 relative abundances can be increased by a factor of between 1 and 3. For 3 of the sources, Mon R2, DR 21 and OMC 2, this would be sufficient to reconcile the abundances from the two models to within a factor of 3, though for S 255 and DR 21(OH), discrepancies of ~ 5 would still remain.

The disagreement between relative molecular abundance estimates between the two models occurs because, for given values of n_{H_2}, X_{HCO^+}, Δv and r, the predicted value of R_{int} is generally greater for model 2 than model 1 (see Fig. 5). The reason for this probably lies in a combination of radiative transfer and relative dilution effects. For a homogeneous LVG clump (model 1), the apparent clump size is the same in the $J = 4 - 3$ transitions of both isotopes. However, for a microturbulent clump (model 2), the apparent size is likely to be smaller for the $H^{13}CO^+$ line. This is because the observed radiation from each clump comes from a characteristic optical depth of about unity, corresponding to a point nearer the clump centre for the less abundant isotope. This implies a smaller apparent clump size and, because the clumps are smaller than the beam, a consequently smaller prediction for the contribution to the integrated flux in the $H^{13}CO^+$ line. In other words, a value of R_{int} greater than unity is here explained not solely in terms of a low $H^{13}CO^+$ optical depth, but also in terms of different dilution factors for the two isotopic lines. As a result, the value of X_{HCO^+} needed to reproduce the observed values of R_{int} is correspondingly increased relative to that given by model 1. These model dependent effects occur here for the simple case of homogeneous clumps and it seems plausible that they would be more pronounced for clumps having internal density and abundance gradients. A more thorough investigation of these model dependent effects, which have serious implications for our ability to estimate reliable relative abundances from molecular line observations, is currently underway (Richardson and Avery, in preparation).

The above analysis has taken no account of the differences in line profile shape observed for some of the sources e.g. the self absorption in DR 21(OH). It is clear that a model consisting of identical homogeneous clumps with no material in between is likely to be an oversimplification of the real structure of a cloud core. In reality, the clumps are unlikely to be identical, and will probably contain local gradients in density, relative molecular abundance and temperature. However one would require a much more complete set of observational data to enable these to be specified uniquely. In particular, and in view of the model dependence of the derived quantities discussed above, we stress the importance of resolving the spatial and kinematic structure of individual clumps with high resolution submillimetre telescopes. In addition to estimating clump sizes and velocity widths, such observations would enable *qualitative* differences in line profiles from individual clumps to be observed directly, and would, for example, allow a distinction to be made between models 1 and 2. An example of this is shown in Fig. 7, in which we show the predicted line profiles of the model 2 solution for Mon R2. Each profile has been convolved with an appropriate gaussian telescope beam: the Nobeyama 45 m for $J = 1 - 0$ and the James Clerk Maxwell Telescope for $J = 4 - 3$. *A prominent self reversal is predicted in the $J = 4 - 3$ line, but not in $J = 1 - 0$* (nor is it observed in our $J = 1 - 0$ data). LVG clumps would give no such feature. Shown also (Fig. 7c–d) is the result when a small systematic collapse, corresponding to 0.15 km s^{-1} at the clump edge, is added. The resultant asymmetry in the predicted line profile is much more conspicuous in the higher transition.

3.3. *Alternative excitation mechanisms*

One assumption we have made in the discussion so far is that the HCO^+ transitions are excited purely by collisions with H_2 molecules in the ground rotational state, together with any effects of radiative trapping. In view of the extreme inhomogeneity of these cloud core regions in density, temperature and kinematics,

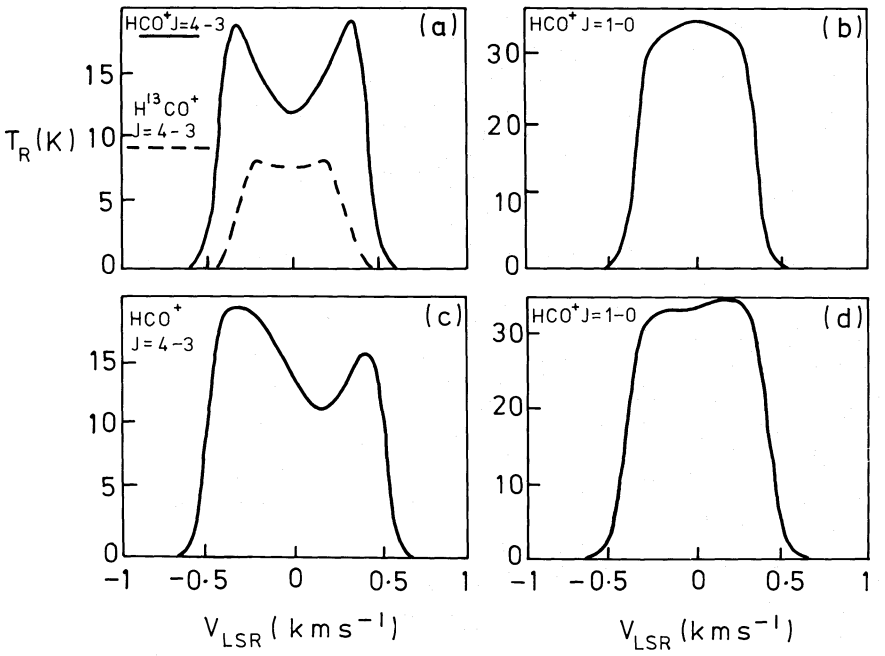

Fig. 7a and b. Predicted line profiles towards a single clump, corresponding to the model 2 solution for Mon R2. The $J = 1 - 0$ and $J = 4 - 3$ lines have been convolved with Gaussian beams appropriate to the Nobeyama and JCMT telescopes respectively. In **c** and **d** the same parameters have been used, except for the addition of a homogeneous systematic collapse, V_{SYS} (km s^{-1}) = $3R$ (pc)

we now briefly consider other mechanisms which might plausibly contribute to line excitation, and give rise to uncertainty in estimated cloud parameters: (1) Excitation by rotationally excited H_2; (2) Excitation via vibrationally excited states of HCO^+ by the infrared continuum radiation field; (3) Ambipolar drift.

3.3.1. Excitation of HCO^+ by collisions with rotationally excited H_2

The first excited state of H_2 ($J = 1$) lies well above (170.5 K) the $J = 0$ level. Nevertheless, this level may still be significantly populated even at relatively low temperatures. The $J = 1$ state is the lowest ortho-H_2 state (nuclear spin 1) and has a statistical spin weighting of 9; so if one assumes H_2 level populations in LTE the fraction of H_2 in the $J = 1$ state will exceed the fraction in the $J = 0$ state for $T > 78$ K. However, this may well underestimate the amount of excited H_2. Ortho/para (i.e. odd J/even J) H_2 are formed in the ratio 3:1. The main mechanism for interconversion (i.e. for taking $J = 1$ H_2 to the ground state) is by proton exchange (Flower and Watt, 1984). This process is relatively inefficient; level populations may not be in LTE in which case there may be an even higher fraction of excited H_2.

Cross sections for H_2 collisions with HCO^+ have therefore been computed for H_2 with both $J = 0$ and $J = 1$ (Monteiro, 1987, unpublished). The HCO^+ -H_2 CI potential of Monteiro (1985) was adapted to permit calculations on H_2 ($J = 1$). Details of the calculation are available from TSM. It was found that, within the range 60–200 cm^{-1} in energy, the H_2 ($J = 1$) and H_2 ($J = 0$) cross sections for almost every transition were well within 35% of each other. Individual cross sections are subject to uncertainties of order 50% from other sources so these differences are not significant. The basic reason for this is that for collisions of H_2 with a charged species, the induction forces resulting from the polarisation of H_2 by the molecular charge will dominate the collision, regardless of the rotational state of H_2.

The results also suggest that in the case of charged molecules, suitably scaled helium rates are representative of H_2 rates whether the H_2 is in the ground state or not. For HCO^+ the rates for collisions with He should be scaled up a factor of 2.5–3.0 to give rates for collisions with H_2. This removes an important source of uncertainty in the collisional rates, and means that the HCO^+-H_2 collisional rates are not an important source of error in cloud modelling.

3.3.2. Radiative excitation by the continuum radiation field

It was suggested by Carroll and Goldsmith (1981) that the near infrared continuum radiation field could play a significant part in exciting rotational molecular transitions via vibrationally excited states. Absorption of an infrared photon can excite a molecule from a particular rotational level J of the ground vibrational state to a vibrationally excited state. This then decays rapidly back to the ground state, either to the same rotational level as before or to level $J + 2$ or $J - 2$. Continuum radiation at the wavelength of an appropriate vibrational transition is expected to provide a significant contribution to the excitation of a rotational transition if the rate of infrared radiative excitation from a particular rotational level exceeds the spontaneous (pure rotational) deexcitation rate from that level i.e.:

$$B_{v,v+1}U \gtrsim A_{J+1,J},$$

where B and A are Einstein coefficients and U is the radiation energy density at the frequency of the vibrational transition (Carroll and Goldsmith, 1981). The relevant vibrational transition of HCO^+ is at a wavelength of 11.3 μm (Rogers and Hillman, 1982) which corresponds to the fundamental bending mode of the molecule, and has a spontaneous emission coefficient $A_{v+i,v}$ (calculated from Rogers and Hillman, 1982) of 1.53 s^{-1}. For the $J = 4 - 3$ transition, $A_{4-3} = 3.8\,10^{-3}$ s^{-1}. Hence we estimate that radiative excitation becomes important if:

$$J_\nu \gtrsim 9\,10^{13} \text{ Jy/sterad}.$$

One can attempt to estimate whether the local radiation intensity is likely to be high enough from observed 11.3 μm fluxes, making allowances for dilution effects and extinction. In the context of a clumpy model we may estimate the average optical depth at 11.3 μm from our estimated 370 μm optical depths. Assuming a λ^{-2} emissivity law from 370 μm to 250 μm and a λ^{-1} variation from 250 μm to 11.3 μm (Hildebrand, 1983; Makinen et al., 1985), the 11.3 μm optical depth $\tau_{11.3}$ along an average line of sight is $\sim 48\,\tau_{370}$. Since τ_{370} is typically ~ 0.1 (see Table 2), values for $\tau_{11.3}$ of ~ 5 (through the whole cloud) are suggested. We assume the observed 11.3 μm continuum to have been subject to attenuation through half this optical depth, a value which, within the errors, is consistent with the typical optical depths of ~ 1–2 as deduced from the 9.7 μm dust absorption feature towards Mon R2 (Beckwith et al., 1976). Hence we deduce that typical observed flux densities of $\sim 7\,10^{12}$ Jy/sterad should be observed, over the HCO^+-emitting material.

The observed infrared fluxes towards our sources do not appear to be sufficient. For Mon R2, the peak 10 μm intensity is $\sim 3\,10^9$ Jy/sterad (Beckwith et al., 1976). From 20 μm mapping of DR 21 (Richardson et al., 1986) and photometry by Wynn-Williams et al. (1974), peak 11.3 μm flux densities of $\sim 1\,10^{10}$ Jy/sterad are suggested, which again is not sufficient. The observed fluxes for S 255, OMC-2 and DR 21(OH) fall short of the required values by even greater margins.

By way of qualification, we note that the shortfall between the observed and required 11.3 μm fluxes could be reduced and probably eliminated by embedding the 11.3 μm emission deep within dense clumps, thereby increasing the optical depth at this wavelength by as much as was required to remove the discrepancy. However, such a model would appear to be somewhat contrived since there seems no reason to suppose that 11.3 μm hot spots would necessarily occur in the centres rather than towards the edges of the clumps. The presently available evidence, therefore, would tend to exclude infrared radiative pumping as a significant contributor to the excitation of the HCO^+ $J = 4 - 3$ transition.

3.3.3. Excitation by ion drift

Clumps in a cloud core are moving in a magnetic field which may be typically < 1 mG. For example, Knapp and Brown (1976) estimated an upper limit of $B < 0.4$ mG in Mon R2. Under the conditions of low ionisation which exist here, a relative velocity will in general exist between the charged species (which tend to be tied to the magnetic field lines) and the neutral species. The question arises as to whether the relative velocity between the HCO^+ ions and the H_2 molecules might suffice to excite the HCO^+ $J = 4 - 3$ transition. For appreciable excitation we require

$$\langle \sigma v \rangle n_{H_2} > A\beta,$$

where β is the photon escape probability. The quantity v would normally be interpreted as a thermal velocity, the collision cross section σ being averaged over a Maxwellian velocity distribution. However, if the relative ion-neutral drift velocity v_{in} exceeded typical thermal values v_{th} (typically $\lesssim 1\,\mathrm{km\,s^{-1}}$), then the extra collisional excitation could mimic the effect of a density $Kn_{H_2}v_{in}/v_{th}$, where K is a numerical factor containing any variation in collisional cross section with collision energy. An estimate of v_{in} can be obtained by considering a conglomeration of clumps with a dispersion of velocities undergoing "collisions" which are mediated by ion-neutral drag forces. Elmegreen (1985) suggests that v_{in} can be estimated by equating the ion-neutral drag force with the inertial force on a clump. Substituting typical values of the relevant parameters, suggested either by Elmegreen (1985) or this work, it is easy to obtain relative drift speeds v_{in} of up to a few $\mathrm{km\,s^{-1}}$, which is indeed significantly large, although a wide range of estimates can be obtained by using different assumed electron densities.

A more detailed picture of molecular line emission from such dense regions (Draine and Roberge, 1982, see also Draine, 1985) attributes it to emission from magnetohydrodynamic shocks. Within a C-type magnetic shock, relative velocities $\sim 10\,\mathrm{km\,s^{-1}}$ can occur between the ions and neutrals over typical distances $\sim 10^{17}$ cm where the temperature is several thousand K. Here, high energy collisions are likely to enhance the emission by a mixture of direct excitation of the rotational transition and indirect excitation via the vibrationally excited levels. For a thermalised and optically thin line of constant excitation temperature T between all levels we have

$$\int T_R\,dV = T\tau\,\Delta V = \frac{8\pi^3\mu^2 2hB^2(J+1)^2 X n_{H_2} L}{3\,10^5 k^2 T}$$

$$= 1.9\,10^{-11}(J+1)^2 X n_{H_2} L/T \quad \mathrm{K\,km\,s^{-1}},$$

where L is the linear extent of the region along the line of sight.

Assuming there to be a single layer of shocked material filling the beam, and taking $X_{HCO+} \sim X_e = 10^{-8}$, $n_{H_2} = 10^5\,\mathrm{cm^{-3}}$ and $L = 5\,10^{16}$ cm, we derive an integrated intensity of

$$\int T_R\,dV \sim 1.5\,10^4/T \quad \mathrm{K\,km\,s^{-1}},$$

and an optical depth (assuming $\Delta V \sim 10\,\mathrm{km\,s^{-1}}$) of $\sim 1.5\,10^3/T^2$.

We thus find that it is easy to account for appreciable HCO^+ intensities by such a mechanism. However, the magnitude of this ambipolar drift effect is sensitive to so many parameters whose values are unknown that it is not possible at present to assess its significance with any degree of accuracy, though it can by no means be excluded as an important contribution to the molecular excitation. If it is, it should be detectable by high resolution mapping in transitions of similar characteristic density of both ionic and neutral species. For example, maps of cloud cores in the transitions HCN $J = 4 - 3$, CS $J = 7 - 6$ and HCO^+ $J = 4 - 3$ might all be expected to reveal a complex spatial/velocity structure, but if this mechanism was important, the HCO^+ mapping would be expected to show features at displaced velocities. In fact something of the sort is seen in our $J = 1 - 0$ data, in which the velocity gradient across the disc of Mon R2 is greater for the HCN line. It must be admitted though that the present data have inadequate signal-to-noise to demonstrate the effect unequivocally. In any case, the effect would probably be more evident in the higher submillimetre transitions which preferentially sample the densest regions where the level of ionisation is likely to be lower and v_{in} correspondingly higher.

4. Conclusions

We have mapped the molecular cloud cores DR 21(OH), Mon R2, and OMC-2 in the $J = 4 - 3$ transition of HCO^+, together with observations at selected positions in the same transition of

$H^{13}CO^+$, and, in the case of Mon R2, higher resolution mapping in the $J = 1 - 0$ transitions of HCO^+, HCN and CO.

For OMC-2, there are significant changes in profile shape over distances of $\lesssim 0.1$ pc, indicating the presence of inhomogeneities on this length scale. Towards DR 21(OH), we observe a self reversal in the HCO^+ $J = 4 - 3$ profile, but not in the $H^{13}CO^+$ line. This feature, and the fact that it is redshifted relative to the line centre, constitutes evidence in favour of a systematic infall of material onto the cloud core, though absorption by a foreground cloud is also a possibility.

In Mon R2, small-scale structure is not directly resolved in the $J = 4 - 3$ transition, but is detected in higher resolution observations in the $J = 1 - 0$ transitions of HCO^+, HCN and CO. The high resolution observations show a double peaked structure in the centre of the source, which may be due to a central rotating disc.

These observations have been interpreted, along with previously presented data for S 255 and DR 21, and submillimetre continuum observations, in terms of a clumpy cloud model. Values derived from the observations for the combined spatial and velocity dilution factor F are ~ 0.1 for all the sources. Average hydrogen densities have been estimated for the regions, and also values for the relative HCO^+ abundance. However the latter quantity is sensitive to the details of the radiative transfer assumed for the clumps; a comparison of LVG and microturbulent modelling techniques shows a range of solutions for n_{H_2} and X_{HCO^+} which extend over orders of magnitude depending on the initial assumptions. Higher spatial resolution submillimetre line observations using the new generation of antennae should enable a choice to be made between various radiative transfer models; *for a wide range of likely clump parameters, we predict the detection of self-reversals in HCO^+ $J = 4 - 3$ (and other optically thick molecular transitions) profiles.*

We have also considered the significance of mechanisms other than collisions with ground state H_2 and He in exciting the HCO^+ $J = 4 - 3$ line. We find that although a significant fraction of the H_2 may well be in a rotationally excited state, this does not have a significant effect on the collisional rates. Radiative excitation of the transition by the infrared continuum radiation field in the cloud core is also considered, but we conclude that this is unlikely to contribute appreciably, unless the extinction at 11.3 μm is much greater than is thought to be the case. One mechanism which could be significant for HCO^+, however, is excitation due to the relative velocity between the charged and neutral species (ambipolar diffusion). This could mimic the effect of a higher gas density than in fact exists. The operation of this mechanism should be detectable by future high resolution submillimetre mapping in transitions of both charged and neutral molecules, where it would show up in velocity displacements between corresponding spectral line features.

The aforementioned uncertainties concerning radiative transfer and excitation mechanisms serve to emphasise the importance of resolving the small-scale structure directly, with the next generation of submillimetre telescopes, so that the individual LSR velocities of clumps, together with their velocity and spatial widths, may be determined. A comparison of qualitative features in the profiles of lines of different species and with different optical depths, will in future enable distinctions to be made between different excitation mechanisms and radiative transfer models for cloud cores. At the same time, it should be stressed that the number of interdependent variables playing a part in line excitation is so large in these dense and complex regions that the gradual accumulation of large and complete data sets on selected regions will certainly be necessary.

Acknowledgements. We thank the UKIRT staff for operation of and assistance at the telescope. We are grateful to SERC for travel grants and funding of the millimetre/submillimetre wave astronomy and receiver development programme at QMC. The Japanese Ministry of Education and SERC are thanked for support of the Japan/UK collaboration. The Monte Carlo modelling program used for part of this work was originally developed by Dr. Lorne Avery, currently at the Herzberg Institute, Ottawa, Canada. We thank the referee, Dr. M. Walmsley, for his helpful comments on the paper.

References

Avery, L.W.: 1983, Monte Carlo Radiative Transfer Program
Beckwith, S., Evans, N.J., Becklin, E.E., Neugebauer, G.: 1976, *Astrophys. J.* **208**, 390
Carroll, T.J., Goldsmith, P.F.: 1981, *Astrophys. J.* **245**, 891
Cunningham, C. A.: 1982, Ph.D. thesis, University of London
Draine, B.T., Roberge, W.G.: 1982, *Astrophys. J.* **259**, L91
Draine, B.T.: 1985, in *Molecular Astrophysics*, NATO Advanced Research Workshop, Reidel, p. 295
Elmegreen, B.G., 1985, in *Nearby Molecular Cloud*, IAU Regional Meeting, Toulouse, ed. G. Serra, Springer Berlin Heidelberg New York, p. 52
Evans, N.J.: 1978, in *Protostars and Planets*, ed. Gehrels, T., University of Arizona Press, p. 153
Fischer, J., Sanders, D.B., Simon, M., Solomon, P.M.: 1985, *Astrophys. J.* **293**, 508
Flower, D.R., Watt, G.D.: 1984, *Monthly Notices Roy. Astron. Soc.* **209**, 25
Gatley, I., Becklin, E.E., Matthews, K., Neugebauer, G., Penston, M.V., Scoville, N.Z.: 1974, *Astrophys. J.* **191**, L121
Goldreich, P., Kwan, J.: 1974, *Astrophys. J.* **189**, 441
Harvey, P.M., Campbell, M.F., Hoffman, W.F.: 1977, *Astrophys. J.* **211**, 786
Harvey, P.M., Joy, M., Lester, D.F., Wilking, B.A.: 1986, *Astrophys. J.* **300**, 737
Hildebrand, R.H.: 1983, *Quart. J. Roy. Astron. Soc.* **24**, 267
Knapp, G.R., Brown, R.L.: 1976, *Astrophys. J.* **204**, 21
Krisciunas, K., Sandell, G., Duncan, W.D., Richardson, K.J., White, G.J.: 1987, *Bull. Am. Astron. Soc.* **19**, 1093
Kutner, M.L., Ulich, B.L.: 1981, *Astrophys. J.* **250**, 341
Loren, R.B.: 1981, *Astrophys. J.* **249**, 550
Makinen, P., Harvey, P.M., Wilking, B.A., Evans, N.J.: 1985, *Astrophys. J.* **229**, 341
Monteiro, T.S.: 1985, *Monthly Notices Roy. Astron. Soc.* **214**, 419
Richardson, K.J., White, G.J., Gee, G., Griffin, M.J., Cunningham, C.T., Ade, P.A.R.A., Avery, L.W.: 1985, *Monthly Notices Roy. Astron. Soc.* **216**, 713
Richardson, K.J., White, G.J., Phillips, J.P., Avery, L.W.: 1986 (Paper I), *Monthly Notices Roy. Astron. Soc.* **219**, 167
Rogers, J.D., Hillman, J.J.: 1982, *J. Chem. Phys.* **77**, 3615
Smith, J., Lynch, D.K., Cudaback, D., Werner, M.W.: 1979, *Astrophys. J.* **234**, 902
Thronson, H.A., Gatley, I., Harvey, P.M., Sellgren, K., Werner, M.W.: 1980, *Astrophys. J.* **237**, 66

Thronson, H.A., Thompson, R.I.: 1982, *Astrophys. J.* **254**, 543
Thronson, H.A., Harper, D.A., Keene, J., Loewenstein, R.F., Harvey, M., Telesco, C.M.: 1978, *Astron. J.* **83**, 492
White, G.J., Avery, L.W., Richardson, K.J., Harten, R.H.: 1986, *Astrophys. J.* **302**, 701
White, G.J., Phillips, J.P., Watt, G.D.: 1981, *Monthly Notices Roy. Astron. Soc.* **197**, 745
White, R.E.: 1977, *Astrophys. J.* **211**, 744
Williams, D.A.: 1986, *Quart. J. Roy. Astron. Soc.* **27**, 64
Wynn Williams, C.G., Becklin, E.E., Neugebauer, G.: 1974, *Astrophys. J.* **187**, 473
Wynn Williams, C.G., Genzel, R., Becklin, E.E., Downes, D.: 1984, *Astrophys. J.* **281**, 172

Note added in proof: Observations directly resolving clumpy structure in DR21(OH) in the 800 μm continuum, using the James Clerk Maxwell Telescope with an angular resolution of 15″, have recently been reported by Krisciunas et al. (1987). These reveal at least 3 separate condensations within a 1 arc min radius of the nominal central position.